Published in final edited form as:
Dev Cell. 2014 December 8; 31(5): 586–598. doi:10.1016/j.devcel.2014.10.006.

Crimpy enables discrimination of pre and postsynaptic pools of a BMP at the Drosophila NMJ

Rebecca E. James[1], **Kendall M. Hoover**[1], **Dinara Bulgari**[4], **Colleen N. McLaughlin**[1], **Christopher G. Wilson**[2], **Kristi A. Wharton**[3], **Edwin S. Levitan**[4], and **Heather T. Broihier**[1,*]

[1]Department of Neurosciences, Case Western Reserve University School of Medicine, Cleveland, OH, 44106, USA

[2]Department of Pediatrics, Case Western Reserve University School of Medicine, Cleveland, OH, 44106, USA

[3]Department of Molecular Biology, Cell Biology, and Biochemistry, Brown University, Providence, RI, 02912, USA

[4]Department of Pharmacology and Chemical Biology, University of Pittsburgh, Pittsburgh, PA, 15261, USA

Summary

Distinct pools of the BMP Glass bottom boat (Gbb) control structure and function of the Drosophila neuromuscular junction. Specifically, motoneuron-derived Gbb regulates baseline neurotransmitter release, while muscle-derived Gbb regulates NMJ growth. Yet how cells differentiate between these ligand pools is not known. Here we present evidence that the neuronal Gbb-binding protein Crimpy (Cmpy) permits discrimination of pre and postsynaptic ligand by serving sequential functions in Gbb signaling. Cmpy first delivers Gbb to dense core vesicles (DCVs) for activity-dependent release from presynaptic terminals. In the absence of Cmpy, Gbb is no longer associated with DCVs and is not released by activity. Electrophysiological analyses demonstrate that Cmpy promotes Gbb's pro-neurotransmission function. Surprisingly, the Cmpy ectodomain is itself released upon DCV exocytosis, arguing that Cmpy serves a second function in BMP signaling. In addition to trafficking Gbb to DCVs, we propose that Gbb/Cmpy co-release from presynaptic terminals defines a neuronal pro-transmission signal.

Introduction

Growth factors regulate morphological and electrophysiological attributes of synapses. In Drosophila, the BMP pathway regulates neuromuscular junction (NMJ) development and function. In the traditional view, the pathway acts in a retrograde direction to coordinate pre

*author for correspondence (heather.broihier@case.edu).

and postsynaptic growth (Aberle et al., 2002; Marques et al., 2002; McCabe et al., 2004; McCabe et al., 2003). However, the pathway regulates more than morphological expansion —BMP pathway mutants also exhibit profound deficits in active zone organization, baseline neurotransmitter release, and synaptic homeostasis. These phenotypes suggest distinct functions for BMP signaling at the NMJ. Indeed, tissue-specific rescue experiments demonstrate that pro-growth and pro-transmission functions are at least partially separable (Goold and Davis, 2007; McCabe et al., 2003). While muscle-specific expression of the BMP ligand Glass bottom boat (Gbb) rescues NMJ morphology in *gbb* mutants, it does not rescue baseline neurotransmission. Neuron-specific Gbb expression is required for normal baseline neurotransmitter release (Goold and Davis, 2007). These data raise the possibility of distinct ligand pools at the NMJ. How are pre and postsynaptic pools of Gbb distinguished?

We previously found that Crimpy (Cmpy) prevents motoneuron-derived Gbb from driving excessive growth at the NMJ (James and Broihier, 2011). Cmpy was identified in a screen for motoneuron-expressed genes and codes for a single-pass transmembrane protein that physically interacts with Gbb. It has sequence homology to the vertebrate transmembrane BMP-binding protein Crim1 (Cysteine-rich in motoneurons-1) (Kolle et al., 2000; Kolle et al., 2003). Loss of Cmpy results in NMJ overgrowth, which is rescued by knockdown of Gbb in motoneurons. Thus, neuronal Gbb drives excessive NMJ growth in *cmpy* mutants. Since neuronal Gbb normally promotes neurotransmitter release, the finding that it promotes NMJ growth in *cmpy* mutants suggested a possible transformation of presynaptic Gbb from a pro-neurotransmission to a pro-growth signal.

To shed light on the role of Cmpy in Gbb regulation, we set out to characterize the presynaptic Gbb pool. In general, proteins are secreted from neurons via one of two major secretory routes: the constitutive secretory pathway (CSP) and the regulated secretory pathway (RSP) (Vazquez-Martinez et al., 2012; Zhang et al., 2010). Vesicles in the CSP spontaneously fuse with the plasma membrane to release their contents. In contrast, vesicles in the RSP undergo regulated Ca^{2+} exocytosis in response to neuronal activity. These pathways bifurcate in the trans Golgi network where proteins destined for the RSP are packaged into dense core vesicles (DCVs) and trafficked to the synapse for activity-dependent release. In the absence of specialized sorting signals/cofactors delivering proteins to the RSP, they are shunted into the CSP for constitutive release (Chen et al., 2005; Lou et al., 2005).

We find that neuronal Gbb is normally trafficked to presynaptic terminals at the NMJ. Levels of presynaptic Gbb are proportional to levels of Cmpy, and Cmpy and Gbb associate with dense core vesicles (DCVs). Arguing that Cmpy delivers neuronal Gbb to DCVs for Ca^{2+}-regulated release, presynaptic Gbb release is absolutely dependent on both synaptic activity and Cmpy. These data provide evidence that Cmpy is a DCV sorting receptor for Gbb. The proposed transformation of presynaptic Gbb from pro-neurotransmission to pro-growth signaling in *cmpy* mutants suggests that Cmpy marks the pro-neurotransmission pool. In support of this hypothesis, Cmpy is necessary for the ability of presynaptic Gbb to fully rescue neurotransmitter release in *gbb* mutants. Moreover, we provide evidence that the Cmpy ectodomain is secreted following nerve depolarization, arguing that Cmpy serves

sequential functions in synaptic BMP signaling. We propose that Cmpy first delivers Gbb to DCVs and is then co-released with Gbb to define a presynaptic pro-neurotransmission signal.

Results

Gbb and Cmpy physically interact and colocalize in presynaptic terminals

Cmpy is a single-pass transmembrane protein (Fig. 1A) that co-immunoprecipitates with Gbb in S2 cells (James and Broihier, 2011). Providing evidence for a direct interaction, we mapped the Gbb-binding domain to Cmpy's C-terminus in a yeast two-hybrid analysis. These biochemical experiments revealed proteolytic processing of Cmpy (James and Broihier, 2011). We detected both full-length Cmpy protein and a C-terminal Cmpy fragment whose molecular weight suggested a cleavage site immediately C terminal to the transmembrane domain (arrow in Fig. 1A). To define Cmpy function *in vivo*, we set out to test if Cmpy and Gbb interact in neurons. To this end, we generated a 6×Myc C-terminal epitope-tagged Cmpy transgene (Cmpy-Myc). Cmpy-Myc is functional as it rescues NMJ overgrowth in *cmpy* nulls (Table S1). On blot, we detect a prominent 39 kDa protein in larval brain lysates corresponding to full-length Cmpy-Myc (Fig. 1B). Anti-Myc antibodies also reproducibly detect a low abundance 31 kDa protein whose size is consistent with the Cmpy cleavage product detected in S2 cells (asterisks in Fig. 1B; James and Broihier, 2011).

We tested whether Cmpy and Gbb are in a physical complex in neurons by co-expressing Cmpy-Myc and Gbb-HA pan-neuronally and assaying if they co-immunoprecipitate in larval brain lysates. We utilized a Gbb transgene tagged with a single internal HA epitope (Gbb-HA). The processing and signaling activity of Gbb-HA is comparable to that of untagged Gbb in cultured cells (Akiyama et al., 2012). *In vivo* activity of Gbb-HA was established in two contexts. First, wing disc expression via A9Gal4 drives blistering phenotypes identical to untagged Gbb (data not shown; James and Broihier, 2011). Second, expression of Gbb-HA in motoneurons drives NMJ overgrowth at muscle 4 indistinguishable from untagged Gbb (Table S1; James and Broihier, 2011). Consistent with a Cmpy/Gbb complex, anti-Gbb brings down Cmpy-Myc from larval brain lysates (Fig. 1C). We detect both 31 and 39 kDa Cmpy-Myc forms following immunoprecipitation, arguing that Gbb interacts with both full-length and processed Cmpy. These data from Drosophila neurons are in line with our previous biochemical studies (James and Broihier, 2011) and support both Cmpy processing and a neuronal Cmpy/Gbb complex.

gbb mutants display pleiotropic defects in active zone organization, neurotransmitter release, and NMJ size, demonstrating that Gbb is a critical regulator of NMJ function and morphology (McCabe et al., 2003; Goold and Davis, 2007). Neuron-derived Gbb is necessary for proper neurotransmission, though whether this represents a local function at synaptic terminals has not been investigated. Thus, we analyzed Gbb localization at the NMJ using an anti-Gbb antibody (Dani et al., 2012; Friedman et al., 2013). In agreement with previous studies (Dani et al., 2012; Friedman et al., 2013), Gbb is robustly expressed at the NMJ (Fig. 1D; Fig. S1). Confirming antibody specificity, this expression is reduced in *gbb* loss-of-function (gbb^{1}/gbb^{2}) mutants (Fig. S1). Notably, Gbb is present inside the presynaptic terminal (Fig. 1D; Fig. S1). While Gbb in the presynaptic compartment may be

neuron-derived, it may also represent muscle-derived ligand, as Gbb is present in internalized endosomes (Alborzinia et al., 2013; Kelley et al., 2009; von Einem et al., 2011). To test if at least some presynaptic Gbb arises within the presynaptic neuron, we asked whether presynaptic Gbb levels are increased following neuronal Gbb overexpression. Animals with neuronal Gbb overexpression exhibit elevated levels of presynaptic Gbb (Fig. S1), indicating that neuronal Gbb can be trafficked to presynaptic terminals.

We next investigated whether Cmpy also localizes to presynaptic terminals. To analyze Cmpy subcellular localization *in vivo*, we generated a C-terminal tagged Cmpy-Venus transgene, which is functional as it fully rescues NMJ overgrowth in *cmpy* nulls (Table S1). When expressed in motoneurons, Cmpy-Venus is trafficked to the NMJ (Fig. 1E). A comparison of the presynaptic distributions of Gbb and Cmpy-Venus indicates that while Gbb is expressed more broadly than Cmpy, the two proteins are found in overlapping subcellular presynaptic regions (Fig. 1 D-F).

Gbb at the NMJ is likely derived from both the presynaptic motoneuron and the postsynaptic muscle. To compare subcellular distribution of Cmpy specifically with neuron-derived Gbb, we expressed Gbb-HA in neurons in order to mark the neuronal Gbb pool. As outlined above, Gbb-HA is functional *in vivo* (Akiyama et al., 2012; Table S1). Neuronal Gbb-HA is trafficked to presynaptic terminals (Fig. 1G). Moreover, Cmpy-Venus and Gbb-HA are found in largely coincident presynaptic regions around the bouton periphery (Fig. 1 G-I). Together, these data argue that both Cmpy and Gbb are trafficked to presynaptic terminals and exhibit presynaptic colocalization.

Crimpy promotes trafficking of Gbb to presynaptic terminals

Cmpy regulates Gbb activity and the two proteins colocalize at the NMJ, raising the possibility that Cmpy controls presynaptic Gbb levels. As a test of this hypothesis, we quantified levels of presynaptic Gbb in *cmpy* nulls. Presynaptic Gbb-HA levels are decreased by 50% in the absence of *cmpy* (Fig. 2 A-D, G), arguing that Cmpy promotes the abundance of presynaptic Gbb. To investigate if Cmpy is sufficient to promote levels of presynaptic Gbb, we tested if Cmpy overexpression increases presynaptic Gbb-HA levels. Neuronal overexpression of Cmpy results in a 2.7-fold increase in presynaptic Gbb-HA (Fig. 2 A-B, E-F, H), indicating that Cmpy is also sufficient to elevate presynaptic Gbb levels. To test if Cmpy regulates postsynaptic Gbb levels, we expressed Gbb-HA in muscle and compared the abundance of postsynaptic ligand in wild type and *cmpy* nulls. Levels of postsynaptic Gbb-HA are unchanged in *cmpy* nulls relative to wild type (Fig. S2), arguing that *cmpy* regulates the abundance of presynaptic, but not postsynaptic, Gbb.

To confirm that motoneuronal Gbb-HA reflects the behavior of endogenous Gbb, we quantified presynaptic levels of endogenous Gbb in wild-type, *cmpy* null, and *cmpy*-overexpressing animals. We quantified Gbb levels inside the presynaptic membrane to focus on neuron-derived Gbb. In *cmpy* nulls, levels of Gbb within the presynaptic terminal are reduced 55% relative to wild type (Fig. 2 I-L, O). Consistent with the hypothesis that Cmpy is a dedicated regulator of presynaptic Gbb, Gbb remains highly expressed outside of the presynaptic membrane in *cmpy* nulls—giving Gbb distribution at the NMJ a hollowed-out appearance (Fig. 2 K-L). Moreover, Cmpy is sufficient to increase presynaptic Gbb levels.

Levels of Gbb inside of the presynaptic membrane are increased 29% in animals overexpressing Cmpy in motoneurons relative to wild-type controls (Fig. 2 I-J, M-N, P). Together, these analyses indicate that levels of presynaptic Gbb are proportional to levels of Cmpy.

To determine if Cmpy regulates Gbb trafficking or total Gbb protein levels, we utilized an anti-Gbb antibody that detects endogenous full-length Gbb on immunoblot (Akiyama et al., 2012). Gbb is synthesized as a 55 kDa precursor protein (Gbb-Pre) that is proteolytically processed to generate mature ligand (Akiyama et al., 2012; Umulis et al., 2009; Walsh et al., 2010). We detect comparable levels of Gbb-Pre in wild type and *cmpy* nulls in brain lobes, ventral ganglia, and body wall (Fig. S3), arguing that *cmpy* does not regulate levels of Gbb precursor protein in these tissues. Thus, Cmpy likely controls synaptic BMP signaling at the level of Gbb trafficking.

Crimpy traffics Gbb to dense-core vesicles (DCVs)

We next sought to elucidate the nature of the neuronal Gbb pool. An established mechanism for presynaptic release of neuropeptides and neurotrophins is via exocytosis of DCVs in response to neuronal activity (Vazquez-Martinez et al., 2012; Zhang et al., 2010). In this case, secreted proteins are packaged into DCVs, which are trafficked to presynaptic terminals and released following Ca^{2+} influx. Mammalian TGFβ family members are trafficked to secretory vesicles and subject to activity-dependent release (Lacmann et al., 2007; Specht et al., 2003), raising the possibility that Cmpy segregates Gbb to DCVs. We first investigated whether Gbb and Cmpy are likely present in DCVs. If so, the proteins are predicted to colocalize with a DCV marker such as fluorescent protein-tagged Atrial natriuretic factor (Anf) (Rao et al., 2001). We find that Cmpy-Venus and Gbb-HA display marked overlap with Anf-mOrange in presynaptic terminals, with all three proteins found predominantly around the bouton perimeter (Fig. 3 A-F). As an essential test of the hypothesis that Cmpy delivers Gbb to DCVs, colocalization of Anf-mOrange and Gbb should be lost in *cmpy* null mutants. Presynaptic accumulation of Gbb is reduced in *cmpy* mutants, so we focused on those *cmpy* mutant NMJs with appreciable presynaptic Gbb. Gbb-HA is no longer significantly associated with Anf-mOrange at these NMJs (Fig. 3 G-I), arguing that Cmpy directs Gbb to DCVs.

In Drosophila, type III boutons on muscle 12 secrete neuropeptides and have been estimated to have nine-fold more DCVs than type Ib boutons (Atwood et al., 1993; Bulgari et al., 2014; Jia et al., 1993; Loveall and Deitcher, 2010). If Gbb-HA and Cmpy-Venus are associated with DCVs, they should be enriched in this bouton type. We find that Gbb-HA and Cmpy-Venus strongly localize to type III boutons (Fig. S4). Moreover, *cmpy* is necessary and sufficient for Gbb-HA trafficking to this terminal (Fig. S4). These data are consistent with the type Ib bouton analysis and provide evidence that Cmpy traffics Gbb to DCVs. To ensure that endogenous Gbb also associates with DCVs, we investigated whether Gbb is also present at type III terminals. Indeed, Gbb is expressed at peptidergic type III terminals in wild type (Fig. 3 J-K). In *cmpy* mutants, Gbb localization to type III terminals is nearly abrogated (Fig. 3 L-M), consistent with an essential role for Cmpy in DCV localization of Gbb.

Activity-dependent Gbb release requires Crimpy

DCVs undergo exocytosis in response to Ca^{2+} influx. If Gbb is present in DCVs, it should be released during nerve stimulation. Thus, we stimulated motoneurons with high K^+ saline and measured levels of Gbb-HA in presynaptic terminals post stimulation. Presynaptic Gbb-HA levels are decreased 58% after high K^+ stimulation relative to unstimulated controls (Fig. 4 A-E). Consistent with Ca^{2+}-dependent release, release is blocked by removing extracellular Ca^{2+} (Fig. 4E). Indeed, removing extracellular Ca^{2+} slightly increases Gbb-HA levels, perhaps reflecting presynaptic buildup of Gbb-HA. As a second test of activity-dependent Gbb-HA secretion, we induced synaptic activity in motoneurons using the blue light-activated cation channel, Channelrhodopsin-2 (ChR2). We exposed larvae expressing ChR2 and Gbb-HA in motoneurons to blue light. Following depolarization, Gbb-HA levels are decreased in presynaptic terminals 43% relative to controls (Fig. 4F). This finding is consistent with decreased Gbb-HA levels following high K^+ stimulation and suggests that Gbb-HA is released by neuronal activity. We next tested whether Cmpy is required for presynaptic release of Gbb. In the absence of Cmpy, Gbb-HA does not localize to DCVs and is not predicted to be subject to activity-dependent exocytosis. In accordance with our model, presynaptic Gbb-HA levels are unchanged following high K^+ stimulation in the absence of Cmpy (Fig. 4G). These data indicate that Cmpy is essential for activity-dependent release of Gbb-HA, arguing that Cmpy delivers Gbb to a Ca^{2+}-regulated secretory pool.

We next assayed whether levels of endogenous presynaptic Gbb decrease following activity. Consistent with the analysis of Gbb-HA, levels of endogenous Gbb are subject to a 26% Ca^{2+}-dependent decrease inside the presynaptic compartment following high K^+ stimulation (Fig. 4 H-L). We propose that total Gbb levels are not reduced as dramatically as neuronal Gbb-HA because the presynaptic terminal also likely contains internalized muscle-derived Gbb by virtue of trans-synaptic pro-growth signaling (Alborzinia et al., 2013; Kelley et al., 2009; von Einem et al., 2011). We next asked whether Gbb levels in presynaptic terminals decrease following stimulation in the absence of Cmpy. We find that the activity-dependent decrease of total Gbb depends on Cmpy, as presynaptic levels of Gbb are unchanged in *cmpy* nulls (Fig. 4 M-Q). Together, these findings argue that activity-dependent Gbb release requires Cmpy.

If presynaptic Gbb is released from DCVs, Gbb-HA levels outside the presynaptic membrane should increase following neuronal activity. Conventional immunofluorescence protocols did not consistently reveal extracellular Gbb-HA (Fig. 4 A-D). To permit its visualization, we optimized an extracellular staining protocol (see Materials and Methods) and increased synaptic delivery of Gbb-HA via Cmpy overexpression. To quantify release, we calculated mean pixel intensity outside of the HRP-positive presynaptic terminal and within a 2.5 μM perimeter surrounding it. We find a 55% increase in Gbb-HA levels within this domain in K^+ stimulated animals relative to non-stimulated controls (Fig. 4 R-V). Demonstrating Ca^{2+} dependence, no increase is observed following high K^+ stimulation without Ca^{2+} (Fig. 4V). These data indicate that Gbb is released in response to synaptic activity.

To further investigate the model that Gbb is released from DCVs, we tested if Gbb-HA release is blocked by the insect-specific Ca^{2+} channel antagonist Plectreurys toxin (PLTX) (Branton et al., 1987). While PLTX blocks small synaptic vesicle exocytosis, it does not block DCV exocytosis (Fig. S5). Thus, if Gbb-HA is released from DCVs, its release will be insensitive to bath application of PLTX. Indeed, PLTX has no effect on Gbb-HA release (Fig. S5), arguing that Gbb-HA is released from DCVs. As a final investigation of the Gbb/Cmpy-positive presynaptic compartment, we tested if Cmpy is in recycling synaptic vesicles labeled by uptake of lipophilic dye (Kuromi and Kidokoro, 2005). Following depolarization, Cmpy-Venus and the lipophilic dye FM4-64 do not exhibit appreciable co-localization in presynaptic terminals (Fig. S5). Together, the PLTX and FM4-64 studies indicate that Cmpy and Gbb are not present in small synaptic vesicles. Given that (1) Gbb is subject to PLTX-insensitive activity-dependent release and (2) Cmpy and Gbb colocalize with DCVs in type Ib and type III boutons—we conclude that Cmpy and Gbb are associated with DCVs in presynaptic terminals.

Crimpy promotes the function of neuron-derived Gbb in synaptic transmission

Cmpy prevents neuronal Gbb from acting as a pro-growth signal (James and Broihier, 2011), raising the possibility that *cmpy* mutants exhibit increased pro-growth Gbb signaling at the expense of the normal function of neuronal Gbb in promoting glutamate release. In this case, loss of Cmpy is predicted to result in decreased neurotransmitter release. To test this hypothesis, we measured spontaneous and evoked synaptic potentials in *cmpy* null mutants via intracellular voltage recording. The amplitude and frequency of spontaneous miniature excitatory junction potentials (mEJPs) are not significantly altered in *cmpy* mutants (Fig. 5A-B; Table S2). However, we find a 28% decrease in the amplitude of evoked EJPs (Fig. 5A, C), which is rescued by Cmpy expression in motoneurons (Fig. 5A, C; Table S2). Thus, Cmpy functions presynaptically to promote baseline transmission, in line with its motoneuron expression (James and Broihier, 2011). We calculated quantal content to estimate the number of vesicles released per action potential and find a 30% decrease at *cmpy* NMJs, which is also rescued by neuronal Cmpy expression (Fig. 5D). The 28% reduction in EJP amplitude in *cmpy* nulls is notable given that these mutants display a 52% increase in bouton number at muscle 6/7 (James and Broihier, 2011). The electrophysiological defect suggests that increased NMJ size in *cmpy* nulls does not offset the defect in neurotransmitter release caused by loss of activity-dependent presynaptic Gbb release.

We hypothesized that Cmpy-mediated activity-dependent release of Gbb is required for baseline glutamate release. If so, this activity of neuronal Gbb should require Cmpy. Thus, we asked if loss of Cmpy interferes with the ability of neuronal Gbb to rescue synaptic transmission defects in *gbb* mutants. We first examined neurotransmitter release in *gbb* mutants. Consistent with previous studies (Goold and Davis, 2007; McCabe et al., 2003), we find that evoked EJP amplitudes are decreased 70% in *gbb* mutants compared to controls (Fig. 5E, H, Table S2). Neuronal expression of a wild-type Gbb transgene confers complete rescue of evoked EJPs and quantal content in a *gbb* mutant background (Fig. 5E, H-I; Table S2) confirming a critical function for neuron-derived Gbb in transmission. We next tested if motoneuronal Gbb still rescues baseline neurotransmission in *gbb; cmpy* double mutants.

Removing Cmpy impairs the ability of neuronal Gbb to rescue EJP amplitude and quantal content in *gbb* mutants by 30% (Fig. 5 E, H-I; Table S2) indicating that Cmpy promotes presynaptic Gbb activity. Loss of Cmpy does not, however, abrogate completely the function of neuronal Gbb, raising the possibility of a Cmpy-independent neuronal pool of Gbb.

We also analyzed bouton number in genotypes with neuronal Gbb overexpression. Neuronal Gbb overexpression increases bouton number in both wild-type and *gbb* null backgrounds (Table S3; James and Broihier, 2011). We interpret the ability of neuronal Gbb to increase bouton number to result from non-Cmpy mediated constitutive Gbb secretion from neurons (see Discussion). In accordance with this model, neuronal Gbb does not require Cmpy to drive growth. Instead, we find a trend toward increased bouton number with neuronal Gbb overexpression in *gbb;cmpy* double mutants relative to a *gbb* single mutants (Table S3). These findings suggest that Cmpy-independent Gbb release from neurons drives growth. Moreover, Cmpy overexpression strongly suppresses NMJ overgrowth caused by neuronal Gbb overexpression (James and Broihier, 2011). Together, these results indicate that Cmpy antagonizes neuronal Gbb's growth-promoting activity.

If Cmpy-regulated neuronal Gbb promotes baseline neurotransmission, loss of either *cmpy* or *gbb* is predicted to yield a similar electrophysiological phenotype. While both mutants do have reduced baseline release, *gbb* mutants are more severely impaired than *cmpy* mutants (Fig. 5A, E). However, *gbb* mutant NMJs are also roughly five times smaller than *cmpy* mutant NMJs, making direct phenotypic comparison difficult. To elucidate potential presynaptic functions of *gbb* and *cmpy*, we analyzed synaptic vesicle cycling in the mutants using the lipophilic dye FM1-43 (Kuromi and Kidokoro, 2005). We quantified average pixel intensity across constant numbers of boutons in mutants and controls to exclude differences secondary to bouton number differences (see Experimental Procedures). We find that both *cmpy* and *gbb* mutants display modest defects in synaptic vesicle endocytosis. FM1-43 dye uptake in high K^+ is impaired 24% in *cmpy* mutants (Fig. 6A1, B1, E), and 15% in *gbb* mutants (Fig. 6 C1, D1, E). Subsequent FM1-43 unloading provides a measure of exocytosis and the size of the cycling vesicle pool. By this measure, *cmpy* mutants exhibit a 52% reduction in synaptic vesicle cycling (Fig. 5 A2, B2, F), relative to a 60% reduction in *gbb* mutants (Fig. 6 C2, D2, F). The similarity in synaptic vesicle cycling defects in *cmpy* and *gbb* mutants supports a requirement for Cmpy-mediated Gbb release in synaptic vesicle dynamics.

The Crimpy C-terminus can be released by synaptic activity

Cmpy's vertebrate homolog, Crim1, is processed to generate a secreted ectodomain that binds BMPs (Wilkinson et al., 2003). Following activity-dependent exocytosis and DCV fusion with the plasma membrane, the C-terminal Gbb-binding domain of Cmpy is predicted to lie on the extracellular side of the presynaptic terminal. Moreover, our biochemical studies suggest proteolytic processing of Cmpy (Fig. 1; James and Broihier, 2011), hinting at the possibility of ectodomain shedding. To test this hypothesis, we asked whether C-terminal tagged Cmpy-Venus levels are regulated by synaptic activity. If Cmpy remains associated with the DCV membrane following activity-dependent exocytosis, Cmpy-Venus

would remain on the plasma membrane or on endosomes. On the other hand, if the ectodomain is released, presynaptic Cmpy-Venus levels are predicted to decrease. Thus, we evaluated Cmpy-Venus levels following depolarization. Consistent with activity-dependent release, presynaptic Cmpy-Venus levels are diminished 36% following stimulation relative to unstimulated controls (Fig. 7 A-E). Demonstrating Ca^{2+} dependence, intracellular Cmpy-Venus levels do not decrease following high K^+ stimulation in the absence of Ca^{2+} (Fig. 7E). Secreted Cmpy is clearly apparent following high K^+ stimulation using an extracellular staining protocol (Fig. 7 A-D, F). To quantify release, we calculated mean pixel intensity outside the presynaptic terminal, and within a 2.5 μM perimeter surrounding it. We find a 62% Ca^{2+}-dependent increase in Cmpy-Venus levels within this region in K^+ stimulated animals (Fig. 7F). As with Gbb, Cmpy release is insensitive to PLTX (Fig. S5), supporting DCV-mediated release. These data suggest that Cmpy's C terminus is released in response to synaptic activity.

To investigate in more detail the possibility of Cmpy processing and ectodomain shedding, we studied the behavior of Cmpy's N terminus following stimulation. We generated a Venus N-terminal epitope-tagged Cmpy transgene (Venus-Cmpy), which localizes to presynaptic terminals when expressed in motoneurons (Fig. 7 G-J). It is functional as it rescues overgrowth in *cmpy* null mutants (Table S1). Consistent with Cmpy cleavage and subsequent ectodomain shedding, we do not detect a change in its distribution following stimulation (Fig. 7 G-L), arguing that the N terminus is not released. These experiments provide evidence that Cmpy is processed *in vivo*. Thus, both the Cmpy ectodomain and Gbb are subject to activity-dependent release from presynaptic terminals. To address the hypothesis that the proteins are co-released from presynaptic terminals, we tested if extracellular Gbb and Cmpy can be simultaneously detected using the extracellular staining protocol that was optimized for Gbb detection. Consistent with an extracellular Gbb/Cmpy complex, we find co-release of Gbb and Cmpy following nerve depolarization (Fig. 7 M-P).

Discussion

Crimpy prevents neuronal Gbb from driving excessive NMJ growth (James and Broihier, 2011). To understand Cmpy-mediated regulation of Gbb, we investigated its mechanism of action. We found that Cmpy controls Gbb trafficking to presynaptic terminals, suggesting that it promotes Gbb function at synapses. Indeed, we provide evidence that Cmpy sorts Gbb into an activity-regulated pool that promotes baseline synaptic transmission. These studies suggest a mechanistic explanation for the proposed switch in signaling identity of neuronal Gbb in *cmpy* mutants. We propose that loss of Cmpy results in inappropriate NMJ growth because neuronal Gbb, which is normally destined for DCVs and released with the Cmpy ectodomain, is shunted into the constitutive secretory pathway (CSP). We further propose that in *cmpy* mutants, constitutively secreted neuronal Gbb is misinterpreted by the neuron as muscle-derived pro-growth signal, leading to NMJ overgrowth. This model is consistent with studies of protein trafficking in mammalian neurons, which have defined constitutive secretion as the default secretory pathway. For example, BDNF secretion is regulated by neuronal activity (Lu and Figurov, 1997). Sorting of BDNF into the regulated secretory pathway is mediated by Sortilin and Carboxypeptidase E. Loss of either protein results in BDNF missorting into the constitutive secretory pathway and enhanced constitutive release

(Chen et al., 2005; Lou et al., 2005). Loss of intrinsic sorting signals also leads to missorting, as mutation of a dileucine-like sorting motif in the vesicular monoamine transporter 2 (VMAT2) diverts VMAT2 from the regulated to the constitutive secretory pathway (Krantz et al., 2000). Consistent with the hypothesis that neuronal Gbb is missorted and constitutively released in the absence of Cmpy, we detect abundant extracellular Gbb-HA in the absence of stimulation in *cmpy* nulls (KMH and HTB, unpublished).

Muscle-derived Gbb synchronizes morphological growth of pre and postsynaptic cells, while neuron-derived Gbb regulates neurotransmitter release (Goold and Davis, 2007; McCabe et al., 2003). We found that Cmpy is required for activity-dependent release of Gbb. It is conceivable that either the location or timing of activity-dependent Gbb release at the NMJ is sufficient to define the presynaptic Gbb pool. It is alternatively possible that Gbb in DCVs in the regulated secretory pathway is processed differently than Gbb in the constitutive secretory pathway. In either case, Cmpy-dependent transport of Gbb to the regulated pathway would serve to mark motoneuron-derived Gbb. Further analysis of Gbb release and processing in *cmpy* mutants will define precisely the Cmpy-dependent DCV pool.

These studies suggest that Cmpy serves a second function in BMP signaling. Our data suggest that a cleaved C-terminal fragment of Cmpy may be secreted with Gbb at the NMJ (Fig. 8). Ectodomain shedding of Cmpy is consistent with the identification of a C-terminal cleavage product with Gbb-binding activity (James and Broihier, 2011). In support of this model, the Cmpy C-terminus is itself subject to activity-dependent release. Drosophila Crimpy shares sequence homology with the vertebrate transmembrane protein Crim1 (Cysteine-rich in motoneurons-1) (Kolle et al., 2000; Kolle et al., 2003). Crim1 interacts with BMP4 and BMP7 and is expressed in motoneuron and interneuron populations in the developing spinal cord, though loss-of-function studies have not uncovered its neuronal function. Significantly, Crim1 is subject to a juxtamembrane cleavage that generates a secreted ectodomain that binds BMPs (Wilkinson et al., 2003). Ectodomain shedding of Crim1 is consistent with the proposed secretion of the Cmpy ectodomain and suggests that the proteins serve similar functions. The proposed sequential roles for Cmpy in Gbb trafficking and signaling are also reminiscent of Sortilin's roles in successive aspects of neurotrophin signaling—Sortilin not only delivers BDNF into the regulated secretory pathway but also forms a complex with the $p75^{NTR}$ receptor to drive cell death (Jansen et al., 2007; Nykjaer et al., 2004). Hence, Sortilin enables separation of pro-apoptosis and pro-survival signal transduction cascades (Nykjaer and Willnow, 2012). As an important test of Cmpy's signaling role, it will be critical to establish whether Cmpy cleavage is essential for its function and if a Cmpy-Gbb complex is secreted from neurons. While we detect Cmpy processing and release, it is possible that full-length Cmpy acts as a BMP co-receptor and that Cmpy is cleaved only after its signaling function is complete. Testing for physical interactions between both cleaved and full-length Cmpy and the neuronal BMP receptors may shed light on the relationship between Cmpy processing and its biological activity.

The distinct signaling outcomes of muscle-derived pro-growth signaling and neuron-derived pro-transmission signaling imply at least partially independent molecular cascades. Hence, it should in principle be possible to identify mutants required for growth, and not transmission,

and vice versa. Motoneurons express canonical members of the BMP signal transduction machinery, including the type II receptor Wishful thinking, the type I receptors Saxophone and Thickveins, the R-Smad Mad, and the co-Smad Medea (Aberle et al., 2002; Allan et al., 2003; Marques et al., 2002; McCabe et al., 2004; McCabe et al., 2003; Rawson et al., 2003). Loss-of-function mutations in these genes result in NMJ undergrowth and defective synaptic transmission, suggesting they regulate both synaptic size and strength. However, it is also possible that the transmission defects are secondary to the severe NMJ growth defects in these backgrounds, obscuring the identities of components dedicated to pro-growth signaling. Conversely, genes required specifically for synaptic transmission would not have been identified in large-scale screens for aberrant NMJ morphology. Dissection of the roles of individual BMP signaling components in both muscle and neuron-derived Gbb signaling will be essential to tease apart the signal transduction cascades.

Regarding pathway directionality, firm evidence indicates that the pro-growth pathway acts in a retrograde direction (Goold and Davis, 2007; McCabe et al., 2003); however, the directionality of the pro-transmission pathway is incompletely defined. While an autocrine signaling mechanism provides the most parsimonious explanation for our findings, we cannot rule out a requirement for postsynaptic muscle in pro-transmission signaling. Our data do not exclude the possibility that motoneuron-derived Gbb induces a postsynaptic signal that in turn promotes neurotransmitter release. Given the number and complexity of signaling interactions at the NMJ (Dudu et al., 2006; Fuentes-Medel et al., 2012; Korkut et al., 2013), it will be crucial to test if components of the BMP signal transduction machinery display postsynaptic requirements for neurotransmitter release.

To the best of our knowledge, Crimpy is the first TGFβ sorting receptor identified in any system. BMP/TGFβ ligands regulate plasticity, cognition, and affective behavior in mammals (Krieglstein et al., 2011). Arguing for local and specific synaptic action, mammalian BMP/TGFβ family members are sorted into secretory vesicles and subject to activity-dependent release (Lacmann et al., 2007; Specht et al., 2003). Given clinical interest in targeting synaptic functions of neuromodulators, a mechanistic understanding of Crimpy and its mammalian homologs will be of interest.

Materials and Methods

Fly stocks are listed in Supplemental Experimental Procedures.

Immunoprecipitation

Lysates were immunoprecipitated with mouse anti-Gbb (Gbb-3D6-24, DSHB). The membrane was probed with rat anti-HA at 1:1000 (Roche) and rabbit anti-Myc at 1:300 (Cell Signaling). The experimental method is detailed in Supplemental Experimental Procedures.

Immunohistochemistry

Immunohistochemistry was carried out as previously described (James and Broihier, 2011). Antibodies and extracellular staining methods are specified in Supplemental Experimental Procedures.

High K^+ depolarization and channelrhodopsin-2 light activation paradigms

Larvae were dissected in ice cold PBS then incubated in 90mM K^+ Jan's saline for 5 minutes. Controls were incubated in normal Jan's saline. To test Ca^{2+} dependence, body walls were incubated in 90mM K^+ Jan's saline without Ca^{2+}. Body walls were fixed in Bouin's fixative and processed for immunohistochemistry in the same tube.

For Channelrhodopsin-2 experiments, larvae expressing *UASChR2* and *UASGbb-1×HA* were reared on 100μM all-trans retinal (Sigma-Aldrich)-containing molasses caps with 100μM all-trans retinal yeast paste at 25°C in the dark. Larval body walls in normal Jan's saline were exposed to blue light through a Zeiss Axioplan 2 band pass GFP filter for 5 minutes prior to fixation and processing for immunohistochemistry. To establish that fluorescence through the GFP filter activates ChR2, *ElavGal4* was used to drive ChR2 in postmitotic neurons and contractions of third instar larvae in response to blue light were assayed as described in (Schroll et al. 2006). For PLTX experiments, high K^+ depolarization experiments were carried out as described above, with the addition of 100 nM PLTX (Alomone labs) to the 90 mM K^+ Jan's saline.

FM1-43 dye uptake assays and live imaging

FM dye loading was carried out as previously described (Nechipurenko and Broihier, 2012), and is described in detail in Supplemental Experimental Procedures.

Electrophysiology

Intracellular recordings were obtained from muscle 6, segment A2–A4 of female third instar larvae in 1.0mM Ca^{2+} HL3 using a Multiclamp 700A (Axon Instruments); data was filtered at 0-2 kHz and digitized at 10k samples/sec using a Digidata 1322A (Axon Instruments). Stimulation was carried out with a Master-8 Stimulator (A.M.P.I.) at 0.2 Hz. MiniAnalysis software (Synaptosoft, Inc.) was used to calculate mEJP and EJP amplitudes. Additional detail is provided in Supplementary Experimental Procedures.

Imaging and data analysis

Larval NMJs were imaged on a Zeiss 510 confocal microscope at 63× and 100×. Brightness and contrast were adjusted in Adobe Photoshop CS5. For all experiments comparing levels of fluorescence, larval body walls were stained in the same tube and brightness/contrast were not altered. To normalize Gbb-HA or Cmpy-Venus protein levels, mean fluorescence levels after subtraction of average background were divided by mean HRP fluorescence. For data analysis, groups of means were compared by one-way ANOVA, and pairs of means by the unpaired Student's t-test.

Extended Experimental Procedures

Fly Stocks

Stocks used in this work include: *D42Gal4* (A. DiAntonio), *UASGbb9.1* (B. McCabe), *UAS-Gbb1×HA* (K. Wharton), *UASCmpy(7)* and $cmpy^{\Delta 8}$ (James and Broihier, 2011) and *A9Gal4* (K. O'Conner-Giles). *UASCmpy-Myc*, *UASCmpy-Venus* (C-terminal epitope), *UASVenus-*

Cmpy (N-terminal epitope) transgenic flies were generated by BestGene, Inc. All other stocks were obtained from Bloomington Stock Center.

Immunohistochemistry

The following primary antibodies were used: rabbit anti-Gbb (1:100, K. Broadie and S. Lee), rat anti-HA High Affinity (clone 3F10, Roche Applied Sciences) at 1:100, chicken anti-GFP (Abcam) at 1:400, rabbit anti-RFP (Abcam) at 1:400, rabbit anti-Myc at 1:300 (Cell Signaling), and DyLight-594 anti-HRP (Jackson ImmunoResearch) at 1:500. The following species-specific secondary antibodies were used: Alexa Fluor 488, Alexa Fluor 568, and Alexa Fluor 647 (Invitrogen) at 1:300. For Cmpy-Venus detection in unpermeabilized conditions following high K^+ depolarization, body walls were fixed in 4% paraformaldehyde in PBS. For all other experiments, body walls were fixed with Bouin's fixative.

For extracellular staining, wandering third instar larvae were dissected in ice cold Ca^{2+}-free HL3 (110mM NaCl, 5mM KCl, 10mM $NaHCO_3$, 5mM Hepes, 30mM sucrose, 5mM trehalose, and 10mM $MgCl_2$) on frozen petri dishes with a very thin coating of Sylgard. Larvae were dissected in less than 90 seconds and immediately fixed with Bouin's fixative, then stored in PBS until processing for immunohistochemistry in detergent-free buffer.

FM1-43 and FM4-64 dye uptake assays and live imaging

For the FM 1-43 dye loading experiment, previously published protocols were used (Daniels et al., 2006, Verstreken et al., 2008). In brief, wandering L3 larvae were dissected in HL-3 solution without calcium (110mM NaCl, 5mM KCl, 10mM $NaHCO_3$, 5mM Hepes, 30mM sucrose, 5 mM trehalose, and 10 mM $MgCl_2$; Verstreken et al., 2008). Synaptic vesicles were labeled by incubating the dissected larvae for 5 min in 4μM FM 1-43 dye (Invitrogen) in 90mM K^+ Jan's saline (45mM NaCl, 90mM KCl, 2mM $MgCl_2$, 36mM sucrose, 5mM Hepes, and 2mM $CaCl_2$, pH 7.3; Jan and Jan, 1976). After stimulation, the larvae were washed with ∼50 ml of calcium-free HL-3 over a period of 12 min. Labeled vesicles at NMJ 4 (for *cmpy* mutant experiments) and NMJ 6/7 (for *gbb* mutant experiments) in A2-A5 segments were imaged on an upright microscope (Axioskop 2) with an Achroplan 63× water immersion objective (Carl Zeiss) using calcium-free HL-3 as an immersion medium. For dye unloading, after imaging, body walls were incubated in 90mM K^+ Jan's saline without dye for 5 min, washed with calcium-free HL-3 as above, and imaged.

Images were acquired at room temperature with identical acquisition settings for all analyzed samples in each experiment. Background fluorescence on the muscle was averaged and subtracted from each dye-loaded image (“before”), and the background intensity after dye unloading was normalized to the “before” image for each NMJ. Average FM1-43 labeling intensity within terminal type Ib boutons was quantified in ImageJ for each genotype. The average fluorescence intensity within five terminal type Ib boutons was quantified for the *cmpy* loss-of-function assays. For the *gbb* loss-of-function quantification, the average fluorescence intensity in three terminal type Ib boutons was quantified, since *gbb* mutant NMJs are very small and often do not have contiguous strands with more than three synaptic boutons.

For FM4-64 colocalization with Cmpy-Venus in live tissue, larvae were dissected and body walls were incubated for 5 min in 4μM FM4-64 dye (Invitrogen) in 90mM K^+ Jan's saline (45mM NaCl, 90mM KCl, 2mM $MgCl_2$, 36mM sucrose, 5mM Hepes, and 2mM $CaCl_2$, pH 7.3; Jan and Jan, 1976). After stimulation, the larvae were washed with ∼50 ml of calcium-free HL-3 over a period of 12 min. The body walls were then stretched taut in Vectashield mounting medium (Vector Laboratories), covered with a coverslip, and immediately imaged on an LSM 510 Meta laser-scanning system (Carl Zeiss) confocal microscope at 100×.

Molecular Biology

Co-immunoprecipitation of Cmpy-Myc and Gbb-HA from brains: 120 ventral nerve cords (VNCs) were dissected from ElavGal4, UASGbb-1×HA, UASCmpy-Myc larvae (experimental) or elavGal4 (control) wandering third instar larvae. VNCs were homogenized in 200 uL cold IP buffer (50 mM Tris pH 7.6, 150 mM NaCl, 1 mM EDTA, 1 % TX-100 (one tablet of complete mini-EDTA-free protease inhibitor cocktail (Roche) was added to 10 mL IP buffer before use)) for 3 min on ice. Extracts were centrifuged for 5 min at 13000 rpm at 4° C. 200 μL total lysate was incubated with 4 μL mouse anti-Gbb O/N at 4° C. 10 μL sample (5% total volume) was removed as “input, before binding”. 100 μL protein G agarose slurry (50 uL resin) was added to the antigen/antibody complex. Incubate with gentle mixing for two hours at 4° C, followed by two hours at RT. Centrifuge and remove supernatant; remove 10 μL sample (5% total volume) as “input, after binding”. Wash bead/antibody complex 3× in cold IP buffer. Spin 2 min at 5000 rpm. Elute proteins by adding 50 μL 2× Laemmli Sample buffer to the resin and incubate 5 min at 95° C. Centrifuge 5000 rpm for 3 min, collect supernatant and run Western blot.

Electrophysiology

Larvae were dissected in Ca^{2+}-free HL3 and recordings were obtained in 1.0mM Ca^{2+} HL3. Data was collected from cells with an input resistance greater than 4 MΩ and resting membrane potential less than -55mV. Sharp electrodes of a resistance between 8–20 MΩ, filled with 3M KCl, were used. Care was taken to ensure that both motorneurons innervating muscle 6 were recruited. Average values for mEJP, EJP, and quantal content were calculated for each recording and then averaged across all recordings. mEJPs were analyzed over a one minute interval, and at least 15 consecutive EJPs were averaged per cell.

Supplementary Material

Refer to Web version on PubMed Central for supplementary material.

Acknowledgments

We thank Nan Liu and Chaoming Zhou for excellent technical assistance. We thank Kendal Broadie, Seungbok Lee, Brian McCabe, the Developmental Studies Hybridoma Bank (DSHB), and the Bloomington Stock Center for reagents and/or stocks. We gratefully acknowledge Alex Kolodkin for his generous support during the final stages of this work. We are grateful to Kate O'Connor-Giles, Andrea Page-McCaw and members of the Broihier lab for thoughtful comments on the manuscript. This work was supported by NIH R56NS055245 and R21NS084202 to HTB.

References

Aberle H, Haghighi AP, Fetter RD, McCabe BD, Magalhaes TR, Goodman CS. wishful thinking encodes a BMP type II receptor that regulates synaptic growth in Drosophila. Neuron. 2002; 33:545–558. [PubMed: 11856529]

Akiyama T, Marques G, Wharton KA. A large bioactive BMP ligand with distinct signaling properties is produced by alternative proconvertase processing. Sci Signal. 2012; 5

Alborzinia H, Schmidt-Glenewinkel H, Ilkavets I, Breitkopf-Heinlein K, Cheng X, Hortschansky P, Dooley S, Wolfl S. Quantitative kinetics analysis of BMP2 uptake into cells and its modulation by BMP antagonists. Journal of Cell Science. 2013; 126:117–127. [PubMed: 23077176]

Allan DW, St Pierre SE, Miguel-Aliaga I, Thor S. Specification of neuropeptide cell identity by the integration of retrograde BMP signaling and a combinatorial transcription factor code. Cell. 2003; 113:73–86. [PubMed: 12679036]

Atwood HL, Govind CK, Wu CF. Differential ultrastructure of synaptic terminals on ventral longitudinal abdominal muscles in Drosophila larvae. J Neurobiol. 1993; 24:1008–1024. [PubMed: 8409966]

Branton WD, Kolton L, Jan YN, Jan LY. Neurotoxins from Plectreurys spider venom are potent presynaptic blockers in Drosophila. The Journal of neuroscience. 1987; 7:4195–4200. [PubMed: 2826721]

Bulgari D, Zhou C, Hewes RS, Deitcher DL, Levitan ES. Vesicle capture, not delivery, scales up neuropeptide storage in neuroendocrine terminals. Proceedings of the National Academy of Sciences of the United States of America. 2014; 111:3597–3601. [PubMed: 24550480]

Chen ZY, Ieraci A, Teng H, Dall H, Meng CX, Herrera DG, Nykjaer A, Hempstead BL, Lee FS. Sortilin controls intracellular sorting of brain-derived neurotrophic factor to the regulated secretory pathway. The Journal of Neuroscience. 2005; 25:6156–6166. [PubMed: 15987945]

Dani N, Nahm M, Lee S, Broadie K. A targeted glycan-related gene screen reveals heparan sulfate proteoglycan sulfation regulates WNT and BMP trans-synaptic signaling. PLoS Genetics. 2012; 8:e1003031. [PubMed: 23144627]

Dudu V, Bittig T, Entchev E, Kicheva A, Julicher F, Gonzalez-Gaitan M. Postsynaptic mad signaling at the Drosophila neuromuscular junction. Current biology. 2006; 16:625–635. [PubMed: 16581507]

Friedman SH, Dani N, Rushton E, Broadie K. Fragile X mental retardation protein regulates trans-synaptic signaling in Drosophila. Disease Models & Mechanisms. 2013; 6:1400–1413. [PubMed: 24046358]

Fuentes-Medel Y, Ashley J, Barria R, Maloney R, Freeman M, Budnik V. Integration of a retrograde signal during synapse formation by glia-secreted TGF-beta ligand. Current Biology. 2012; 22:1831–1838. [PubMed: 22959350]

Goold CP, Davis GW. The BMP ligand Gbb gates the expression of synaptic homeostasis independent of synaptic growth control. Neuron. 2007; 56:109–123. [PubMed: 17920019]

Jansen P, Giehl K, Nyengaard JR, Teng K, Lioubinski O, Sjoegaard SS, Breiderhoff T, Gotthardt M, Lin F, Eilers A, et al. Roles for the pro-neurotrophin receptor sortilin in neuronal development, aging and brain injury. Nature Neuroscience. 2007; 10:1449–1457.

Jia XX, Gorczyca M, Budnik V. Ultrastructure of neuromuscular junctions in Drosophila: comparison of wild type and mutants with increased excitability. J Neurobiol. 1993; 24:1025–1044. [PubMed: 8409967]

Kelley R, Ren R, Pi X, Wu Y, Moreno I, Willis M, Moser M, Ross M, Podkowa M, Attisano L, et al. A concentration-dependent endocytic trap and sink mechanism converts Bmper from an activator to an inhibitor of Bmp signaling. The Journal of Cell Biology. 2009; 184:597–609. [PubMed: 19221194]

Kolle G, Georgas K, Holmes GP, Little MH, Yamada T. CRIM1, a novel gene encoding a cysteine-rich repeat protein, is developmentally regulated and implicated in vertebrate CNS development and organogenesis. Mech Dev. 2000; 90:181–193. [PubMed: 10642437]

Kolle G, Jansen A, Yamada T, Little M. In ovo electroporation of Crim1 in the developing chick spinal cord. Dev Dyn. 2003; 226:107–111. [PubMed: 12508231]

Korkut C, Li Y, Koles K, Brewer C, Ashley J, Yoshihara M, Budnik V. Regulation of postsynaptic retrograde signaling by presynaptic exosome release. Neuron. 2013; 77:1039–1046. [PubMed: 23522040]

Krantz DE, Waites C, Oorschot V, Liu Y, Wilson RI, Tan PK, Klumperman J, Edwards RH. A phosphorylation site regulates sorting of the vesicular acetylcholine transporter to dense core vesicles. The Journal of Cell Biology. 2000; 149:379–396. [PubMed: 10769030]

Krieglstein K, Zheng F, Unsicker K, Alzheimer C. More than being protective: functional roles for TGF-beta/activin signaling pathways at central synapses. Trends Neurosci. 2011; 34:421–429. [PubMed: 21742388]

Lacmann A, Hess D, Gohla G, Roussa E, Krieglstein K. Activity-dependent release of transforming growth factor-beta in a neuronal network in vitro. Neuroscience. 2007; 150:647–657. [PubMed: 17997227]

Lou H, Kim SK, Zaitsev E, Snell CR, Lu B, Loh YP. Sorting and activity-dependent secretion of BDNF require interaction of a specific motif with the sorting receptor carboxypeptidase e. Neuron. 2005; 45:245–255. [PubMed: 15664176]

Loveall BJ, Deitcher DL. The essential role of bursicon during Drosophila development. BMC Dev Biol. 2010; 10:92. [PubMed: 20807433]

Lu B, Figurov A. Role of neurotrophins in synapse development and plasticity. Rev Neurosci. 1997; 8:1–12. [PubMed: 9402641]

Marques G, Bao H, Haerry TE, Shimell MJ, Duchek P, Zhang B, O'Connor MB. The Drosophila BMP type II receptor Wishful Thinking regulates neuromuscular synapse morphology and function. Neuron. 2002; 33:529–543. [PubMed: 11856528]

McCabe BD, Hom S, Aberle H, Fetter RD, Marques G, Haerry TE, Wan H, O'Connor MB, Goodman CS, Haghighi AP. Highwire regulates presynaptic BMP signaling essential for synaptic growth. Neuron. 2004; 41:891–905. [PubMed: 15046722]

McCabe BD, Marques G, Haghighi AP, Fetter RD, Crotty ML, Haerry TE, Goodman CS, O'Connor MB. The BMP homolog Gbb provides a retrograde signal that regulates synaptic growth at the Drosophila neuromuscular junction. Neuron. 2003; 39:241–254. [PubMed: 12873382]

Nykjaer A, Lee R, Teng KK, Jansen P, Madsen P, Nielsen MS, Jacobsen C, Kliemannel M, Schwarz E, Willnow TE, et al. Sortilin is essential for proNGF-induced neuronal cell death. Nature. 2004; 427:843–848. [PubMed: 14985763]

Nykjaer A, Willnow TE. Sortilin: a receptor to regulate neuronal viability and function. Trends Neurosci. 2012; 35:261–270. [PubMed: 22341525]

Rawson JM, Lee M, Kennedy EL, Selleck SB. Drosophila neuromuscular synapse assembly and function require the TGF-beta type I receptor saxophone and the transcription factor Mad. J Neurobiol. 2003; 55:134–150. [PubMed: 12672013]

Specht H, Peterziel H, Bajohrs M, Gerdes HH, Krieglstein K, Unsicker K. Transforming growth factor beta2 is released from PC12 cells via the regulated pathway of secretion. Mol Cell Neurosci. 2003; 22:75–86. [PubMed: 12595240]

Vazquez-Martinez R, Diaz-Ruiz A, Almabouada F, Rabanal-Ruiz Y, Gracia-Navarro F, Malagon MM. Revisiting the regulated secretory pathway: from frogs to human. Gen Comp Endocrinol. 2012; 175:1–9. [PubMed: 21907200]

von Einem S, Erler S, Bigl K, Frerich B, Schwarz E. The pro-form of BMP-2 exhibits a delayed and reduced activity when compared to mature BMP-2. Growth factors (Chur, Switzerland). 2011; 29:63–71.

Wilkinson L, Kolle G, Wen D, Piper M, Scott J, Little M. CRIM1 regulates the rate of processing and delivery of bone morphogenetic proteins to the cell surface. The Journal of Biological Chemistry. 2003; 278:34181–34188. [PubMed: 12805376]

Zhang X, Bao L, Ma GQ. Sorting of neuropeptides and neuropeptide receptors into secretory pathways. Prog Neurobiol. 2010; 90:276–283. [PubMed: 19853638]

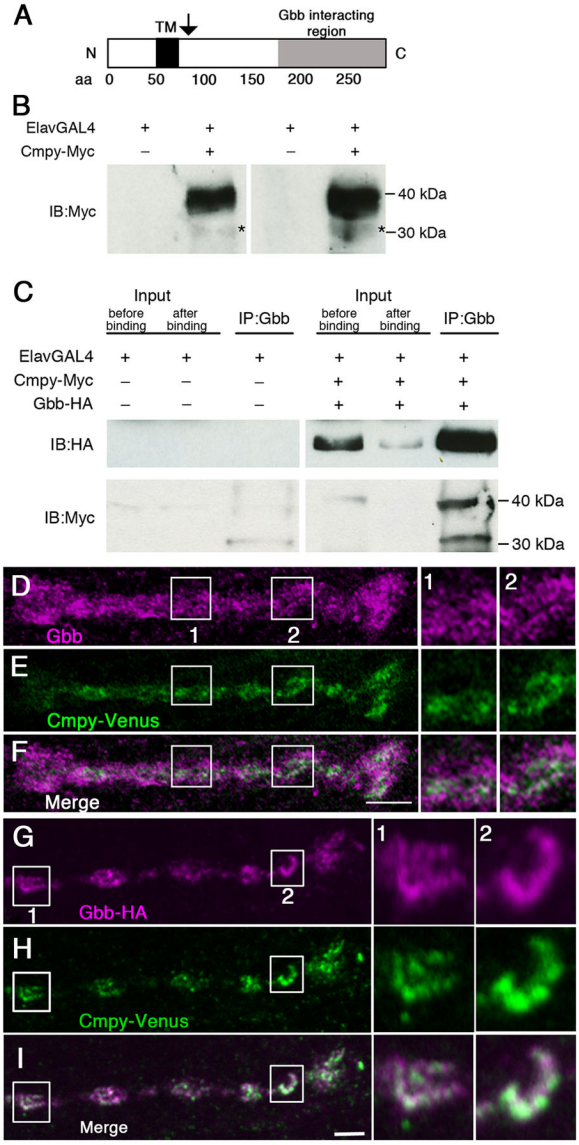

Figure 1. Crimpy and Gbb physically interact and colocalize in presynaptic terminals

(A) Cmpy is a predicted Type II transmembrane protein. TM is the predicted transmembrane domain. Arrow indicates position of proposed proteolytic processing. (B) Two representative immunoblots of third instar ventral nerve cords (VNCs) from *ElavGal4* or *ElavGal4/UASCmpy-Myc* animals. Left blot: 15 VNCs/lane; right blot: 25 VNCs/lane. Full-length Cmpy-Myc is 39 kDa; putative 31 kDa C-terminal Cmpy-Myc cleavage product (asterisk). (C) Co-immunoprecipitation of Gbb-HA and Cmpy-Myc from VNCs of the indicated genotypes. Mouse anti-Gbb antibody was used to immunoprecipitate Gbb-HA followed by Western blotting analysis using Rat anti-HA (top) and Rabbit anti-Myc (bottom) to detect Gbb and Cmpy, respectively. Proteins in the lysate prior to immunoprecipitation (5% of total input) are shown on the left before and after binding to anti-Gbb beads. Anti-Gbb co-immunoprecipitates full-length 39 kDa Cmpy-Myc and a 31 kDa Cmpy-Myc cleavage product. (D-F) Representative confocal images of boutons at

NMJ4 of *D42Gal4, UASCmpy-Venus* larvae stained with anti-Gbb (D) and anti-GFP (E) with the channels merged in (F). Boxes (1) and (2) are magnified to the right of panels (D-F) to demonstrate co-localization of Cmpy-Venus (anti-GFP) and Gbb (anti-Gbb). (G-I) Representative confocal images of boutons at NMJ4 of *UASGbb-HA; D42Gal4/UASCmpy-Venus* larvae stained with anti-HA (G) and anti-GFP (H) with the channels merged in (I). Boxes (1) and (2) are magnified to the right of panels (G-I) to demonstrate co-localization of Cmpy-Venus (anti-GFP) and Gbb-HA (anti-HA). Scale bars are 2 μm.

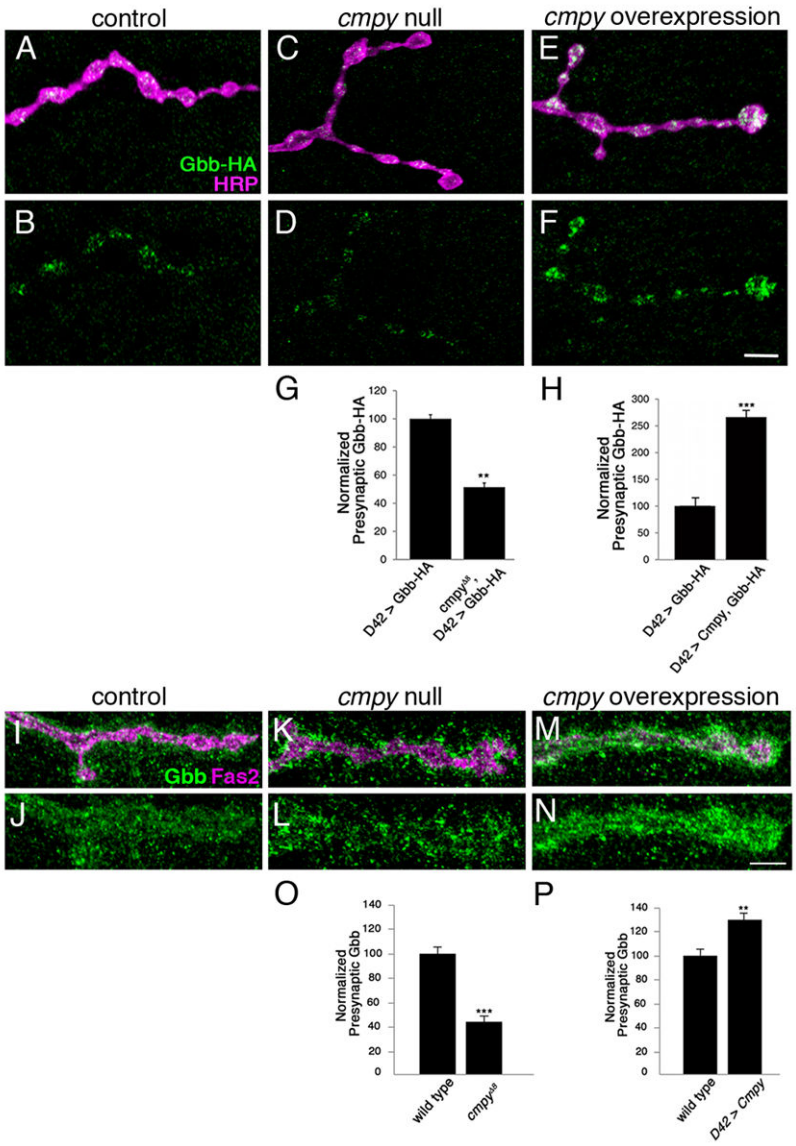

Figure 2. Crimpy promotes trafficking of Gbb to presynaptic terminals

(A-F) Representative confocal images of boutons at NMJ4 of larvae expressing Gbb-HA via D42Gal4 in otherwise wild-type (A,B), *cmpy*$^{\Delta 8}$ homozygous (C,D) and Cmpy overexpression (E,F) backgrounds stained with anti-HA (Gbb-HA) and anti-HRP (neuronal membrane). (G) Quantification of the Gbb-HA/HRP ratio for the indicated genotypes indicates that presynaptic levels of Gbb-HA are reduced two-fold in *cmpy* nulls (n > 25 NMJs). (H) Quantification of the Gbb-HA/HRP ratio for the indicated genotypes indicates that presynaptic levels of Gbb-HA are increased 2.7-fold by Cmpy overexpression (n > 12 NMJs). (I-N) Representative confocal images of boutons at NMJ4 of wild-type (I,J), *cmpy*$^{\Delta 8}$ homozygous (K,L) and *D42Gal4*, *UASCmpy-Venus* (M,N) larvae stained with anti-Gbb (Gbb) and anti-Fas2 (neuronal membrane). (O) Quantification of mean pixel intensity of Gbb inside the presynaptic terminal defined by Fas2 for the indicated genotypes indicates that presynaptic levels of Gbb are decreased more than two-fold in *cmpy* nulls (n = 8 NMJs).

(P) Quantification of mean pixel intensity of Gbb inside the presynaptic terminal defined by Fas2 for the indicated genotypes indicates that presynaptic levels of Gbb are increased 1.3-fold by Cmpy overexpression (n = 8 NMJs). Scale bars are 2 μm. ** $p<0.01$ and *** $p<0.001$; error bars are SEM.

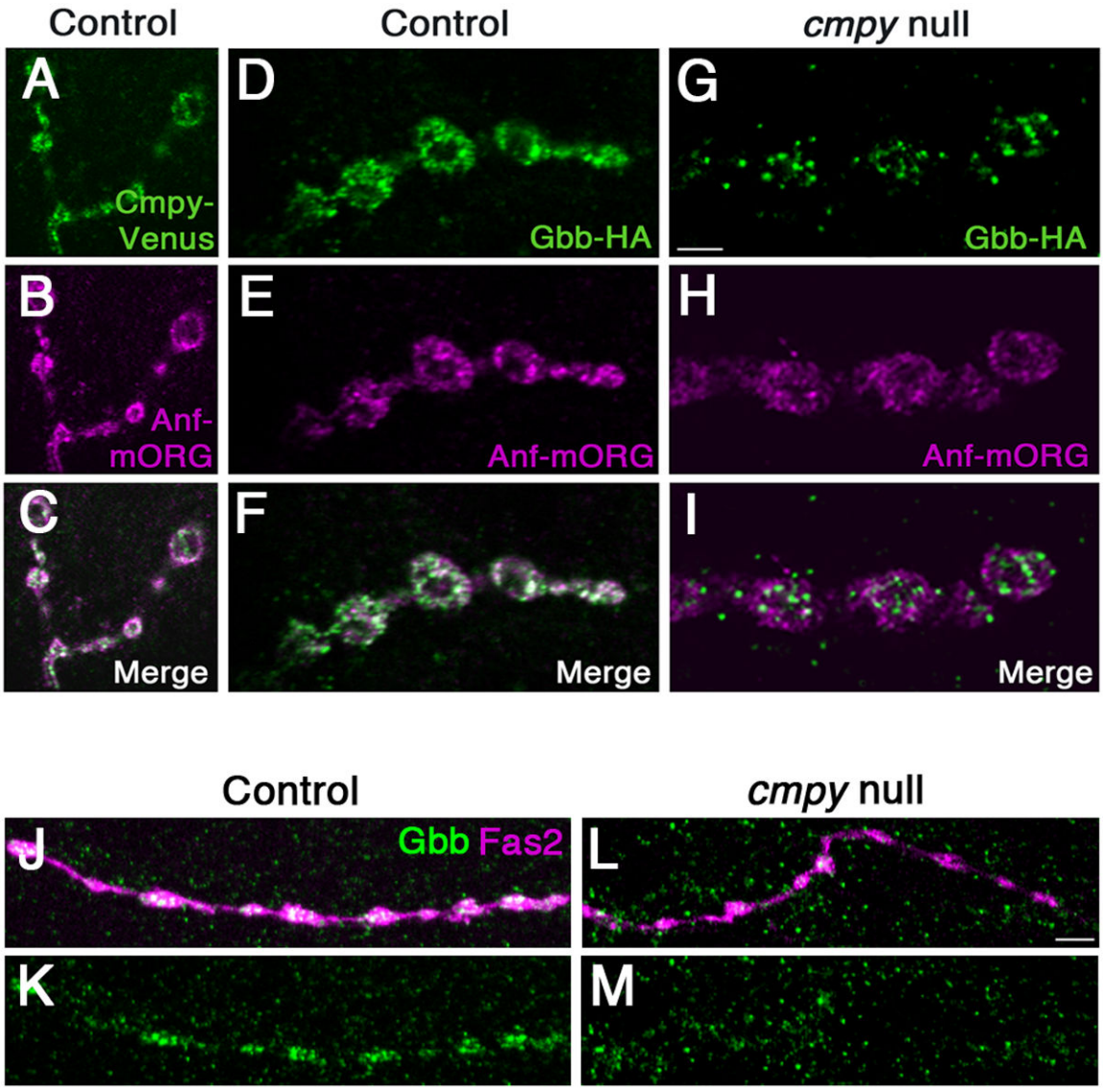

Figure 3. Crimpy traffics Gbb to dense core vesicles

(A-C) Representative confocal images of boutons at NMJ4 of *D42Gal4, UASCmpy-Venus/UASAnf-mOrange* larvae stained with anti-GFP (A), anti-RFP (B), and merged in (C) demonstrate association of Cmpy-Venus (anti-GFP) with Anf-mOrange/DCVs (anti-RFP) in presynaptic terminals. (D-I) Representative confocal images of boutons at NMJ4 in larvae with *Gbb-HA, Anf-mOrange* expressed via *D42Gal4* in an otherwise wild-type background (D-F) and in a $cmpy^{\Delta 8}$ background (G-I) stained with anti-HA (Gbb-HA) and anti-RFP (Anf-mOrange/DCVs). In an otherwise wild-type background, Gbb-HA and Anf-mOrange display extensive co-localization. In $cmpy^{\Delta 8}$ mutants, presynaptic Gbb-HA does not exhibit appreciable co-localization with Anf-mOrange. (J-M) Representative confocal images of type III boutons on muscle 12 in larvae with *Anf-mOrange* expressed via *D42Gal4* in an otherwise wild-type background (J,K) and in a $cmpy^{\Delta 8}$ background (L,M) stained with anti-Gbb (Gbb) and Fas2 (neuronal membrane). In an otherwise wild-type background, Gbb

strongly localizes to type III boutons. In *cmpy*$^{\Delta 8}$ mutants, Gbb does not exhibit appreciable localization in type III boutons. Scale bars are 2 μm.

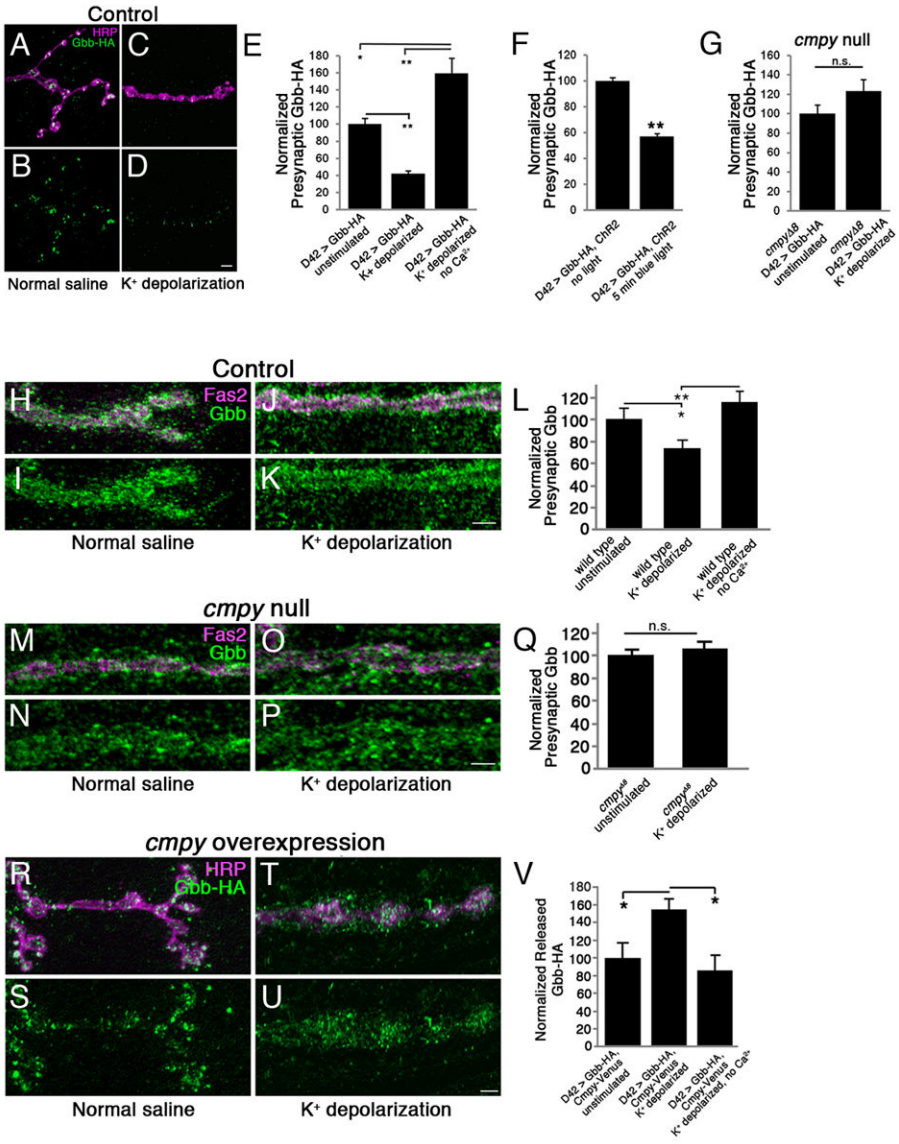

Figure 4. Activity-dependent Gbb release requires Crimpy

(A-D) Representative confocal images of boutons at NMJ4 in *UASGbb-HA; D42Gal4* larvae stained with anti-HRP (neuronal membrane) and anti-HA (Gbb-HA). Before fixation, larvae were incubated for five minutes in normal (A,B) or 90 mM K^+ (C,D) saline. (E) Quantification of the Gbb-HA/HRP ratio in *UASGbb-HA; D42Gal4* larvae for the indicated conditions (n > 50 NMJs for each). High K^+ depolarization results in decreased intracellular Gbb-HA. (F) Quantification of the Gbb-HA/HRP ratio in *UASGbb-HA; D42Gal4/ UASChR2.S*. larvae (n > 40 NMJs for each). ChR2-induced depolarization promotes Gbb release. (G) Quantification of the Gbb-HA/HRP ratio in *UASGbb-HA; D42Gal4, cmpy$^{\Delta 8}$/ cmpy$^{\Delta 8}$* larvae (n > 40 NMJs for each). High K^+ stimulation does not drive Gbb release in *cmpy$^{\Delta 8}$* mutants. Scale bars are 5 μm. * p<0.05, ** p<0.01, n.s. not significant. Error bars are SEM. (H-K) Representative confocal images of boutons at NMJ4 in wild-type larvae stained with anti-Fas2 (neuronal membrane) and anti-Gbb (Gbb). Before fixation, larvae

were incubated for five minutes in normal (H,I) or 90 mM K^+ (J,K) saline. Wild type is Oregon R. (L) Quantification of presynaptic Gbb. Mean pixel intensity of Gbb inside the presynaptic terminal as defined by Fas2 is reduced 25% following stimulation in high K^+ saline. (n = 8 NMJs for each). (M-P) Representative confocal images of boutons at NMJ4 in *cmpy*$^{\Delta 8}$ homozygous larvae stained with anti-Fas2 (neuronal membrane) and anti-Gbb (Gbb). Before fixation, larvae were incubated for five minutes in normal (M,N) or 90 mM K^+ (O,P) saline. (Q) Quantification of presynaptic Gbb as defined in (L). No change is observed following stimulation (n > 9 NMJs for each). (R-U) Representative confocal images of boutons at NMJ4 in *UASGbb-HA; D42Gal4/UASCmpy-Venus* larvae stained with anti-HRP (neuronal membrane) and anti-HA (Gbb-HA). Before fixation, larvae were incubated for five minutes in normal (R,S) or 90 mM K^+ (T,U) saline. (V) Quantification of the released Gbb-HA/HRP ratio. Mean pixel intensity of Gbb-HA outside of presynaptic terminal as defined by HRP, but within a 2.5 μm perimeter surrounding the terminal, is increased 50% following stimulation in high K^+ saline. No increase is observed when Ca^{2+} is removed from the high K^+ buffer. (n = 10 NMJs for each). Scale bars are 2 μm. * $p<0.05$, ** $p<0.01$, n.s. not significant. Error bars are SEM.

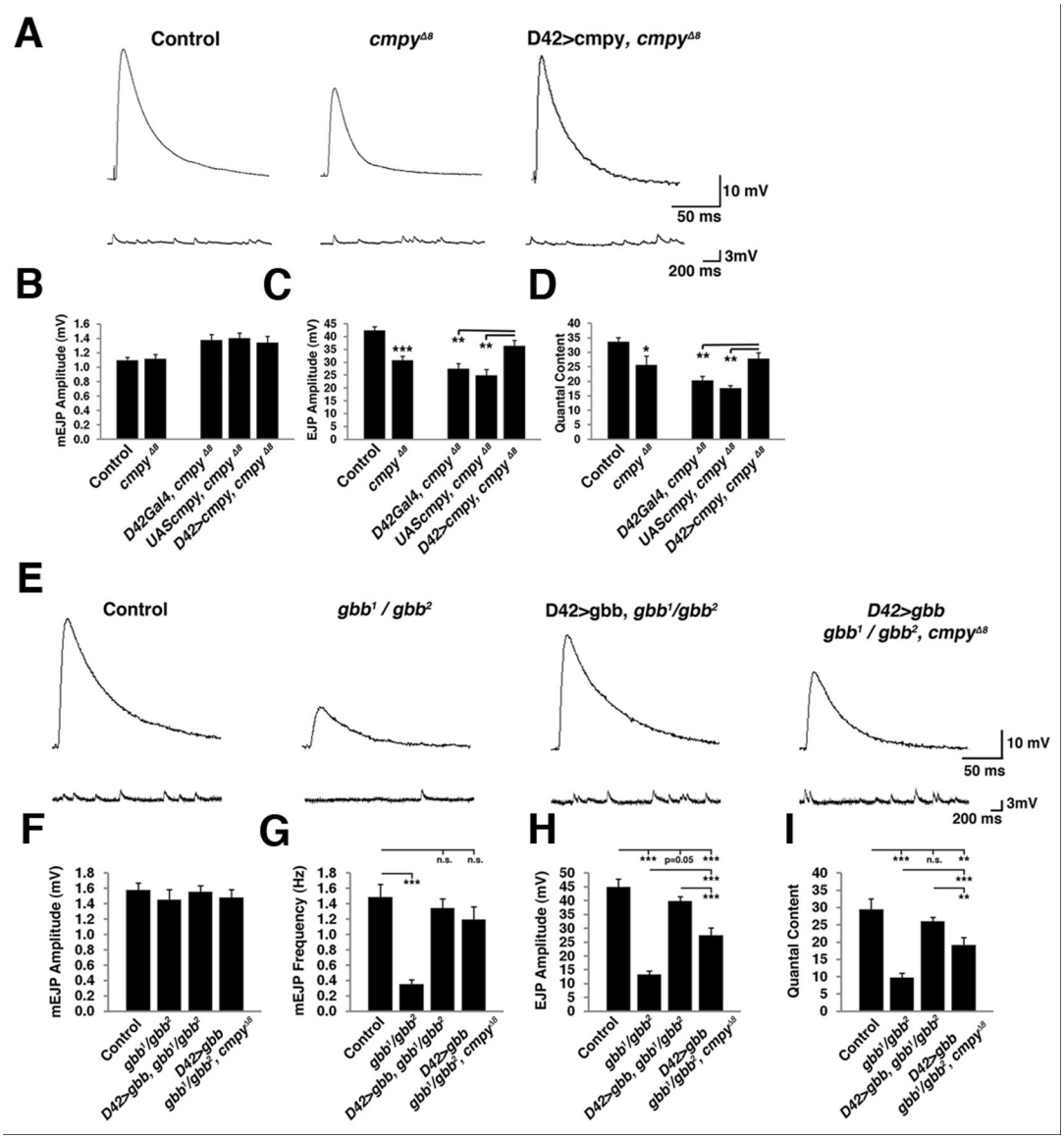

Figure 5. Crimpy promotes the function of neuronal Gbb in synaptic transmission

(A) Representative traces from control (*PBac*^{f01736}/*PBac*^{f02482} = parental line in which *cmpy*$^{\Delta 8}$ deletion was generated), *cmpy*$^{\Delta 8}$ homozygotes, and motoneuron rescue flies (D42Gal4, *cmpy*$^{\Delta 8}$/UASCmpy, *cmpy*$^{\Delta 8}$). Recordings were obtained from muscle 6 of abdominal segments A2-A4 at 1.0 mM extracellular Ca^{2+}. Top traces are representative evoked EJPs and bottom traces are spontaneous EJPs. (B-D) Mean mEJP amplitude, mean EJP amplitude, and quantal content for the indicated genotypes (n = 18 for control, n = 17 for *cmpy*$^{\Delta 8}$ homozygotes, n = 8 for D42Gal4, *cmpy*$^{\Delta 8}$ and UASCmpy, *cmpy*$^{\Delta 8}$ controls, and also for D42Gal4, *cmpy*$^{\Delta 8}$/UASCmpy, *cmpy*$^{\Delta 8}$ rescue). Mean mEJP amplitude is not significantly different for any of the genotypes compared to wild type. Mean EJP amplitude is decreased 28% in *cmpy* nulls and is fully rescued by neuronal expression of Cmpy. (E) Representative traces of evoked (top) and spontaneous (bottom) excitatory potentials from control (Canton-S), *gbb*^{1}/*gbb*^{2} transheterozygotes, *gbb*^{1}/*gbb*^{2}; *D42Gal4*/*UASGbb9.1*, and

gbb^{1}/*gbb*^{2}; *D42Gal4 cmpy*$^{\Delta 8}$/*UASGbb9.1 cmpy*$^{\Delta 8}$ larvae. Recordings were obtained from muscle 6 of abdominal segments A2-A4 at 1.0 mM extracellular Ca^{2+}. (F-I) Mean mEJP amplitude, mean mEJP frequency, mean EJP amplitude, and quantal content for the indicated genotypes (n = 8 for control, n = 10 for *gbb*^{1}/*gbb*^{2}, n = 11 for *gbb*^{1}/*gbb*^{2}; *D42Gal4/UASGbb9.1*, and n = 11 for *gbb*^{1}/*gbb*^{2}; *D42Gal4 cmpy*$^{\Delta 8}$/*UASGbb9.1 cmpy*$^{\Delta 8}$. (F) Mean mEJP amplitude is not significantly different for any of the indicated genotypes compared to wild type. (G) Mean mEJP frequency is reduced 74% in *gbb* null mutants and is fully rescued by motoneuronal *gbb* in the presence and absence of *cmpy*. (H) Mean EJP amplitude is decreased 70% in *gbb* mutants and is rescued to 88% of control levels in *gbb*^{1}/*gbb*^{2}; *D42Gal4/UASGbb9.1* animals. Loss of Cmpy impairs the ability of motoneuronal Gbb to rescue evoked EJPs in *gbb* nulls by 30%. (I) Quantal content is decreased 67% in *gbb* mutants and is rescued by motoneuronal Gbb. Loss of Cmpy impairs the ability of motoneuronal Gbb to rescue quantal content in a *gbb* nulls by 26%. * $p<0.05$, ** $p<0.01$, ***, $p<0.001$, n.s. not significant. Error bars are SEM.

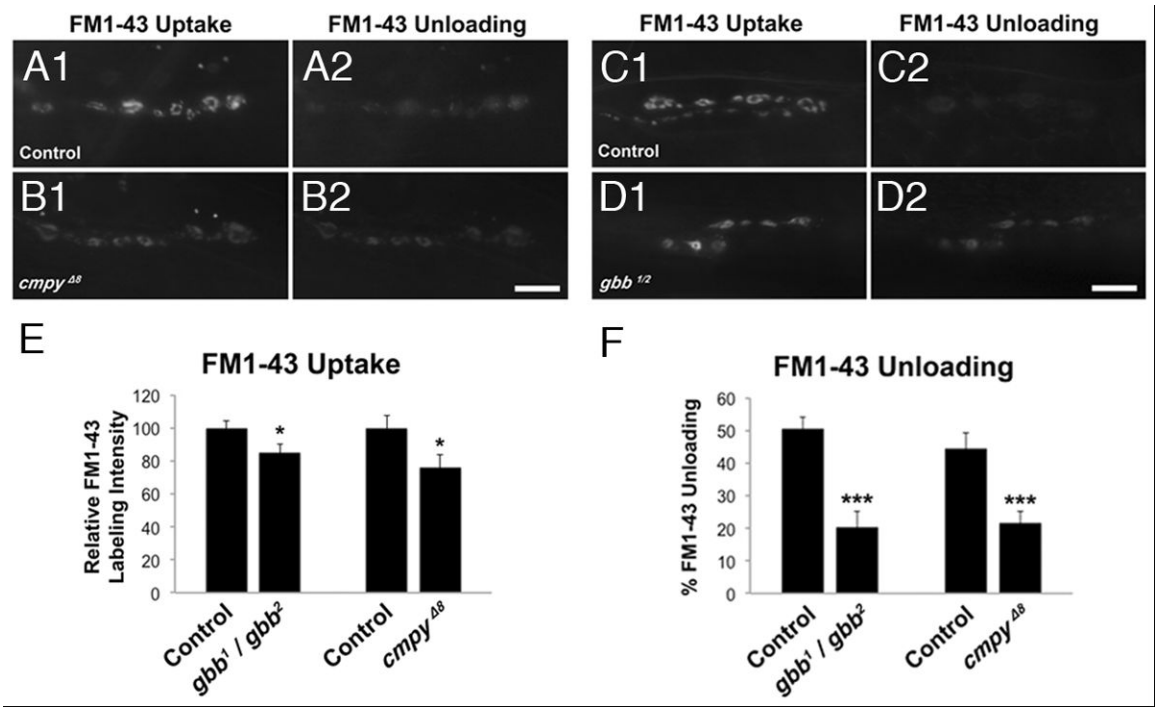

Figure 6. Crimpy and Gbb are comparably required for synaptic vesicle cycling

(A1-D2) Representative images of FM1-43 dye uptake (A1, B1, C1, D1), and dye unloading (A2, B2, C2, D2), after 90mM K^+ depolarization with and without dye in the bath, respectively. Control is heterozygous parental *PBac* elements, $PBac^{f01736}/PBac^{f02482}$ in (A1-A2) and Canton-S in (C1-C2). Scale bars: 10μM. (E) Quantification of normalized FM1-43 labeling intensity after dye uptake for the indicated genotypes. (F) Quantification of the ratio of FM1-43 dye unloading to loading for the indicated genotypes. n > 20 NMJs scored. * $p<0.05$, ***, $p<0.001$, n.s. not significant. Error bars are SEM.

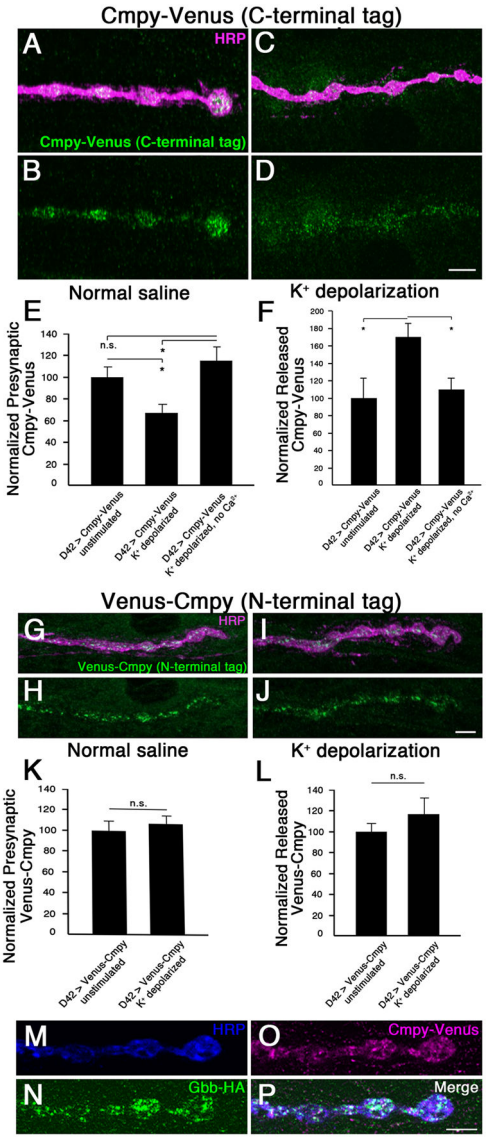

Figure 7. The Crimpy C-terminus can be released by synaptic activity

(A-D) Representative confocal images of boutons at NMJ4 in *D42Gal4/UASCmpy-Venus* (C-terminal epitope tagged) larvae stained with anti-HRP (neuronal membrane) and anti-GFP (Cmpy-Venus). Before fixation, larvae were incubated for five min in normal (A,B) or 90 mM K^+ (C,D) saline. (E) Quantification of the presynaptic Cmpy-Venus/HRP ratio. Mean pixel intensity of presynaptic Cmpy-Venus is reduced 36% following stimulation in high K^+ saline. No reduction is seen when Ca^{2+} is removed from the high K^+ buffer. (F) Quantification of the released Cmpy-Venus/HRP ratio. Mean pixel intensity of Cmpy-Venus outside of presynaptic terminal as defined by HRP, but within a 2.5 μm perimeter surrounding the terminal, is increased 62% following stimulation in high K^+ saline. No increase is observed when Ca^{2+} is removed from the high K^+ buffer. (n > 16 NMJs for each). (G-J) Representative confocal images of boutons at NMJ4 in *UASVenus-Cmpy; D42Gal4*, (N-terminal epitope tagged) larvae stained with anti-HRP (neuronal membrane)

and anti-GFP (Venus-Cmpy). Before fixation, larvae were incubated for five min in normal (G,H) or 90 mM K^+ (I,J) saline. (K) Quantification of the presynaptic Venus-Cmpy/HRP ratio. Mean pixel intensity of presynaptic Venus is unchanged following stimulation. (L) Quantification of the released Cmpy-Venus/HRP ratio as defined in (F). No change is observed following stimulation (n > 12 NMJs for each). (M-P) Representative confocal images of boutons at NMJ4 in *UASGbb-HA/+; D42Gal4/UASCmpy-Venus* larva stained with anti-HA (Gbb-HA), anti-GFP (Cmpy-Venus), and anti-HRP (neuronal membrane). Scale bars: 2 μm. *p<0.05, n.s. not significant. Error bars are SEM.

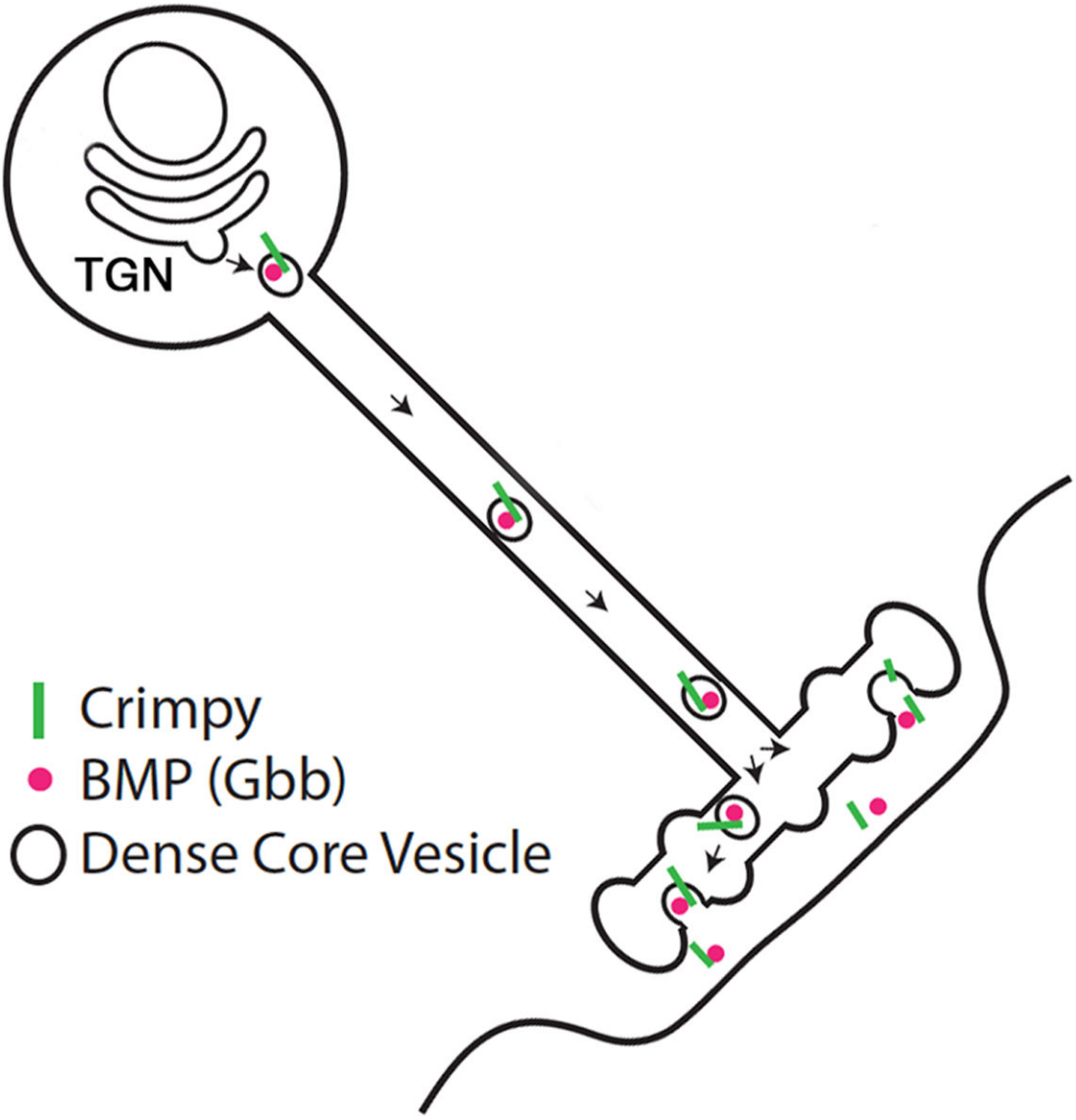

Figure 8. The Crimpy C-terminus and Gbb are released upon synaptic activity

Proposed model for Cmpy-mediated Gbb activity. Cmpy associates with Gbb in the secretory pathway, sorting Gbb into DCVs. DCVs containing Gbb and Cmpy are trafficked to presynaptic terminals. The Cmpy C-terminus and Gbb are released following synaptic activity. We favor the hypothesis that Gbb and Cmpy are co-released in a complex, but we cannot exclude the possibility of independent co-release.